Journal of Electronics and Electrical Engineering
https://ojs.wiserpub.com/index.php/JEEE

Research Article

A High-Power Hybrid-Strip Monopulse Antenna Array for Secondary Surveillance Radars

Ahmed Alieldin*, Alla M. Eid, Amgad A. Salama

The Egyptian Technical Research and Development Centre, Elsayeda Aisha, Cairo 11618, Egypt
E-mail: ahmed.alieldin@alexu.edu.eg

Received: 28 September 2024; **Revised:** 18 December 2024; **Accepted:** 20 December 2024

Abstract: This paper proposes a novel design of a high-power monopulse antenna array for secondary surveillance radars utilized in air traffic control systems. A novel technique of hybrid-strip technology is applied to the antenna array (composed of stripline for the feeding network and microstrip for the antenna elements) to minimize the effect of the transition between the feeding network and antenna elements. The antenna array consists of two identical mirrored halves. Each half is 2 rows × 6 columns. The antenna elements are rectangular microstrip patches with shorting vias while the feeding network is composed of a combination of synthesized stripline dividers/combiners. A backfill antenna along with a control network is utilized to achieve the monopulse technique and sidelobe suppression. The control network is a stripline rat race attached to couplers. The antenna array achieves an excellent monopulse performance at the uplink (1030 MHz) and the downlink (1090 MHz) with a return loss better than 15 dB, a realized gain of 22.2 dBi and two independent Sum and Diff channels with a Sum-to-Diff ratio of 30 dB at the antenna boresight. The antenna array can handle a peak power of up to 2.7 MW for long-range traffic detection and control. Such performance makes the proposed antenna array a perfect candidate for secondary surveillance radar.

Keywords: air traffic control, antenna array, high power, hybrid-strip, monopulse, secondary surveillance radar

1. Introduction

Air traffic control (ATC) aims to guide airborne vehicles safely and efficiently throughout the airspace system. Once an airborne vehicle takes off, it communicates with a ground-based secondary surveillance radar (SSR) to track the progress of the aircraft through the airways system. All systems have similar waveforms and share common frequencies of 1030 MHz for the uplink and 1090 MHz for the downlink. Polarization is always vertical [1, 2, 3].

Scientists and researchers have developed antennas for the SSR systems for decades to meet the requirements of the ATC systems and several designs have been reported. The antenna of an SSR typically has two main beams (Sum and Diff) forming a monopulse technique so that the SSR interrogates and receives replies from the flying aircraft only when it is supposed to (the aircraft is at the antenna boresight) depending on the difference in gains between the Sum and Diff beams (typically within a 9 dB difference in gains between Sum and Diff beams) [4]. However, many other antenna designs have used a third beam of an omnidirectional antenna as a sidelobe suppression (SLS) technique to suppress the communication between the SSR and the flying vehicles through the sidelobes [5, 6, 7].

DOI: https://doi.org/10.37256/jeee.4120255815

Although being efficient, this technique adds complexity not only to the antenna itself but also to the overall SSR system in terms of its transmitter, receiver and/or its signal processing.

The authors in [8] have presented a multilayer antenna array to cover both the uplink and the downlink simultaneously. Later on, in [9], a slotted antenna array for an SSR system with a broad bandwidth was presented. In both the previous designs, two beams (Sum and Diff) were not sufficient to suppress sidelobe communications between SSR and airborne vehicles. The authors in [10] came up with a good idea to improve the SLS by adding a backfill antenna coupled with the Diff beam. Unfortunately, being horizontally polarized and having an implementation unfeasibility limit this design to be practically applicable for SSR systems.

Handling a high transmitted power is also one of the biggest challenges in designing an antenna for SSR. Many practical designs have utilized stripline (SL) technology to build the feeding network of the antenna array so that it can handle high power during transmission [7]. However, when connecting an SL network to a patch antenna designed based on microstrip (MS) technology, many aspects should be taken into account such as the changes in the propagation modes and the discontinuity in the transmission lines (TLs). These aspects may cause severe losses in the propagating signals affecting highly the performance of the antenna array [11]. To overcome these challenges, some techniques have been presented including a vertical coaxial transition from MS to SL and vice versa resulting in a complex multilayer structure [12]. Other designs have utilized a tapered TL to transit between MS and SL which increased the overall size of the structure unnecessarily [13] while others applied a stepped ground plane [14] or coupled lines [15].

In this paper, a novel high-power monopulse antenna array is proposed to be utilized for SSR systems. A novel hybrid-strip (HS) methodology is applied in designing the antenna array to merge the SL and MS technologies while minimizing the transition effects. Moreover, the SLS technique is applied by employing only two beams (Sum and Diff) and utilizing a backfill antenna along with a control network to suppress the sidelobe communications without adding more complexity to the SSR system.

The rest of the paper is organized as follows: Section 2 discusses the methodology of the HS technology, Section 3 presents the design and the principle of operation of the antenna column, Section 4 illustrates the whole antenna array and its feeding network, Section 5 describes the control network, Section 6 proposes the full prototype and its measurements and finally, conclusions are drawn in Section 7.

2. The methodology of the hybrid-strip technology

In this section, the methodology of the hybrid-strip (HS) technology is discussed in details. The HS technology is then applied to designing the proposed antenna array. The methodology starts by discussing the SL and MS technologies and how they are merged to form an HS network.

Impedances (Z_{MS}) and (Z_{SL}) of MS TL and SL TL, respectively, are related to their dimensions and the utilized dielectric material by [16]:

$$Z_{MS} = \frac{120\pi}{\sqrt{\varepsilon_r}\left[\frac{W}{h} + 1.393 + 0.667\ln\left(\frac{W}{h} + 1.444\right)\right]} \tag{1}$$

$$Z_{SL} = \frac{30\pi}{\sqrt{\varepsilon_r}\left(\frac{W}{2h} + 0.441\right)} \tag{2}$$

where ε_r is the relative permittivity of the dielectric material, w is the width of the TL and h is the height of the TL above the ground plane.

By dividing Equation (2) by (1), we get

$$\frac{Z_{SL}}{Z_{MS}} = 0.5\left[1 + \frac{0.6 + 0.667\ln\left(\frac{W}{h} + 1.444\right)}{\left(\frac{W}{h} + 0.882\right)}\right] \tag{3}$$

The relationship derived in (3) can be represented graphically as shown in Figure 1. It is clear from Figure 1 that to connect and match an SL network to an MS network (by obtaining equal matching impedances ($Z_{SL} = Z_{MS}$) at a certain value of w/h) either the width of the TL (w) should be zero (the TL vanishes) or the height h should be extended to ∞. Both cases are unrealistic. However, Z_{SL} may equal Z_{MS} with the same h only if each has its own width (W_{SL} and W_{MS} respectively) as shown in Figure 2. The difference in the widths of W_{SL} and W_{MS} causes discontinuities which result in severe losses in the structure.

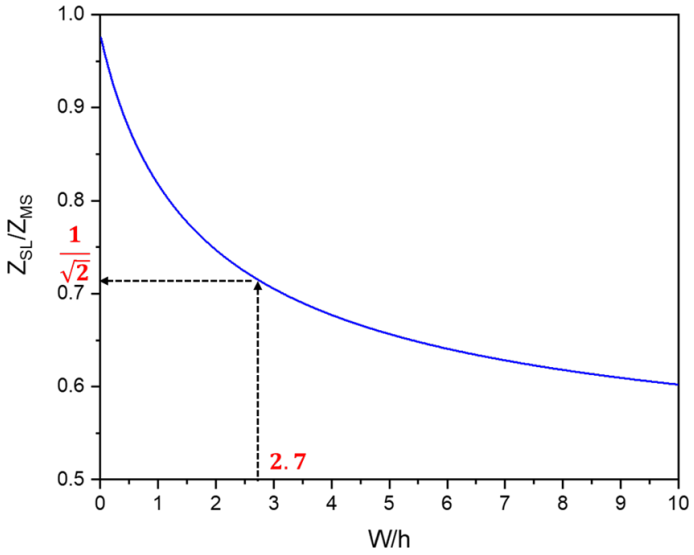

Figure 1. The relation between Z_{SL}/Z_{MS} and w/h

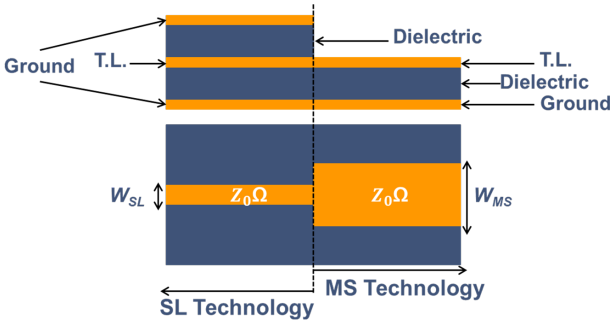

Figure 2. Discontinuity in matched SL and MS networks

To overcome these discontinuities, an HS methodology is adopted where both W_{SL} and W_{MS} are set to the same value (W_{HS}). Of course, in this case, Z_{SL} no longer matches Z_{MS}. Therefore, one of the networks (let's assume the MS network) is tuned by adding a matching network to have an overall input impedance matched with the SL network while both have the same TL width (W_{HS}) as shown in Figure 3a.

For better understanding, let's select from Figure 1 the value where $w/h = 2.7$. In this case, $Z_{SL}/Z_{MS} \approx 1/\sqrt{2}$. So, if the SL network is designed to have a characteristic impedance $Z_{SL} = Z_0$, the MS network should be designed such that its input

TL has a characteristic impedance of $\sqrt{2}Z_0$ while the overall MS network has an input impedance of Z_0 as shown in Figure 3b.

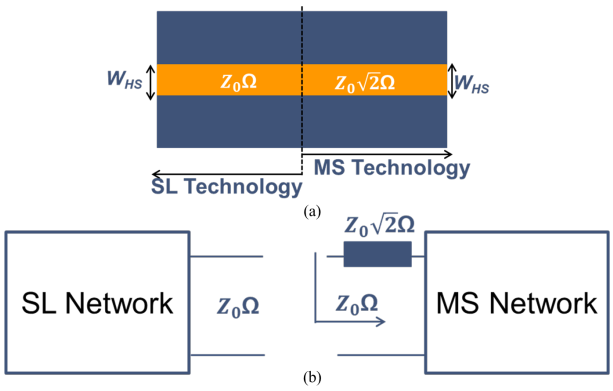

Figure 3. The proposed HS methodology (**a**) layout (**b**) matching technique

3. The proposed antenna column

The antenna column is a two-element MS series-feed linear antenna array. Each element is a patch antenna which consists of a feeding layer, a radiating layer and a shorting via as shown in Figure 4. The feeding layer and the radiating layer are made from an aluminium sheet with a thickness of 1.5 mm, the ground plane is made from an aluminium sheet with a thickness of 3 mm while the via is made from an aluminium rod. The spacing between the two patches is set to λ_0 (where λ_0 is the free space wavelength at the centre frequency 1060 MHz). The patches are designed based on an airgap as a dielectric. The optimized dimensions of the column are tabulated in Table 1.

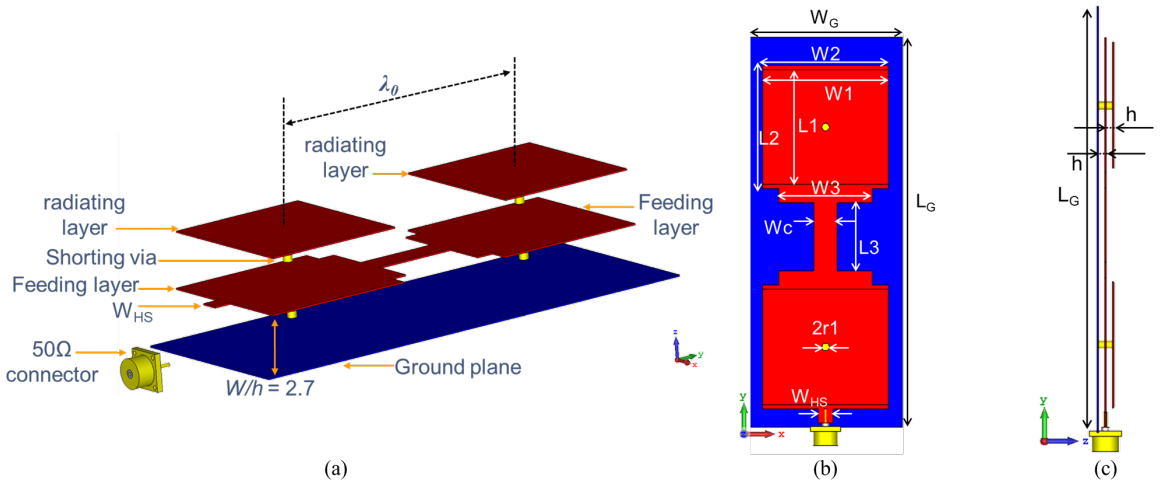

Figure 4. The proposed antenna column (**a**) exploded geometry (**b**) front view (**c**) side view

Table 1. The parameters of the proposed antenna column (in mm)

Parameter	Value	Parameter	Value	Parameter	Value
W_1	135	W_C	25	L_3	73
W_2	135	W_{HS}	16	L_G	415
W_3	100	L_1	123	r_1	4
W_G	165	L_2	132	h	5.75

To design the antenna column, firstly, the value of W_{HS}/h was set to 2.7 so that Z_{MS} equals 70.7 Ω (Z_0 = 50 Ω). The feeding layer is directly connected to the excitation port while the radiating layer is excited by the capacitive coupling (C_C) due to its proximity to the feeding layer [17]. A shorting via is then added to the structure to introduce an inductive loading (L_V) to the patch antenna [18]. This inductive loading in addition to the capacitive coupling creates a resonance. The diameter and the position of the shorting via are selected and optimized such that the resonance occurs at the desired frequencies when the input impedance of the whole antenna column is Z_0 as in Figure 5.

The simulated return loss and realized gain of the antenna column are shown in Figure 6. The antenna column achieves a return loss of better than 20 dB at the desired frequencies. The realized gain of the antenna column is around 11.5 dBi.

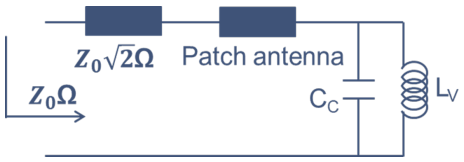

Figure 5. The equivalent circuit of the proposed antenna column.

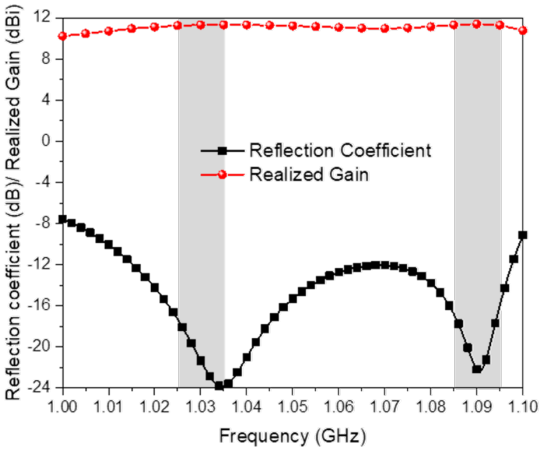

Figure 6. The Simulated reflection coefficient and realized gain of the proposed antenna column

The simulated radiation patterns at the E-plane (YZ-plane) and H-plane (XZ-plane) at 1030 MHz and 1090 MHz are presented in Figure 7. The proposed antenna column has HPBWs of 32° and 72° at the E-plane and H-plane respectively.

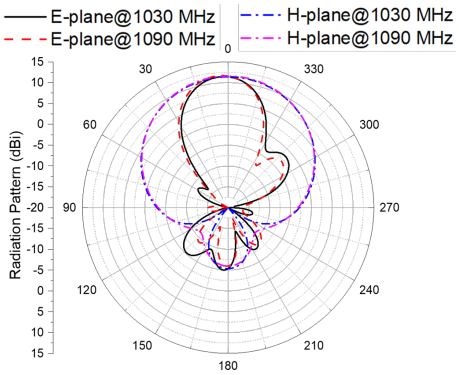

Figure 7. The simulated radiation patterns of the proposed antenna column

4. The proposed antenna array

The proposed antenna array consists of two identical mirrored halves (*A1* and *A2*). Each half contains six replicas of the proposed antenna column where each column is placed along the Y-axis and the columns are spaced along the X-axis by an interspacing of $0.8\lambda_0$ forming a 2×12 planar array as shown in Figure 8.

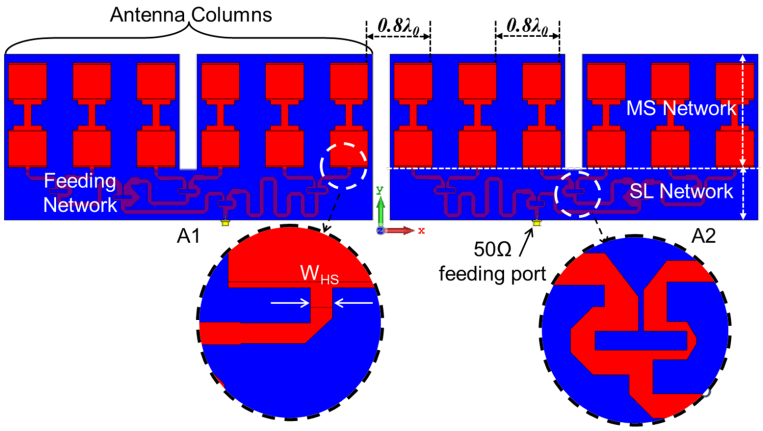

Figure 8. The proposed antenna array

The six columns in each half are fed by a feeding network designed based on SL technology with air gaps as a dielectric. The feeding network and its ground planes are made from aluminium sheets with thicknesses of 1.5 and 3 mm respectively.

The feeding network consists of a combination of 5 unequal power dividers to achieve a synthesized weight distribution to minimize the sidelobe level (SLL) of the antenna array. The weights are distributed such that the feeding network delivers its maximum power to the middle ports and gradually decreases outwards. However, its output ports are all in-phase. The complex insertion losses (magnitudes and phases) and the normalized weight distribution of the feeding network are shown in Figure 9. The input and output TLs of the feeding network have a width of W_{HS} while the thickness of the air gap between the feeding network and any of the two opposite ground planes is h. So, the input and output ports are matched at $Z_{SL} = 50\ \Omega$. Hence, there is no change in the TL widths at the junction between the feeding network (SL network) and the antenna column (MS network). Therefore, the transition effect due to the discontinuity is almost eliminated and the goal of the HS technology is achieved.

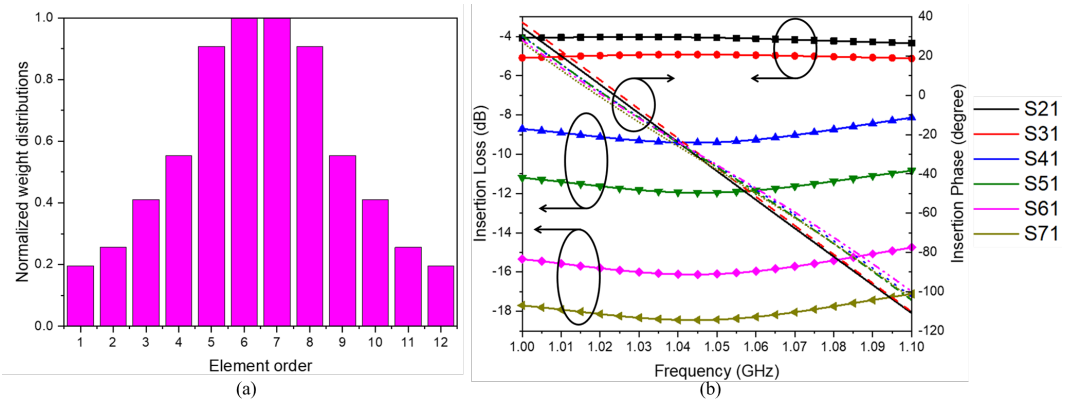

Figure 9. The feeding network (**a**) weight distributions (**b**) insertion losses and phases

To mechanically support the feeding network, maintain the uniformity of the airgaps and confirm the electrical connection between the two ground planes, cylindrical aluminium spacers are added between the two ground planes. Moreover, cylindrical Polytetrafluoroethylene (PTFE) spacers (with a relative permittivity $\varepsilon_r \approx 2.1$) are introduced to keep the feeding network centred between the airgaps.

5. The control network

To achieve a monopulse technique with two beams (Sum and Diff), a control network is utilized. The control network is designed based on SL technology. It consists of two main parts: a rat-race and directional couplers. The function of the rat-race is to provide two equal-amplitude (in-phase and out-phase) signals in order to form the Sum and Diff beam patterns respectively. The main function of the directional coupler is to feed a backfill antenna to improve the coverage of the Diff beam and guarantee its full coverage over the sidelobes of the Sum beam in all azimuth angles (especially at the back lobe). The backfill antenna is typically an antenna column which is placed behind the antenna array at a distance of $0.25\lambda_0$ facing backwards (toward the negative Z axis).

5.1 *The proposed rat-race*

The proposed rat-race is shown in Figure 10 and its dimensions are tabulated in Table 2. Its network is designed based on SL technology with air gaps as a dielectric. The network is made of copper with a thickness of 35 μm and printed on a hexagonal-shaped FR-4 laminate with a thickness of 0.8 mm and a relative permittivity $\varepsilon_r \approx 4.3$ while the ground planes are made from an aluminum sheet with a thickness of 3 mm. The thickness of the air gaps between the network and any of the two opposite ground planes is h. To keep the uniformity of the air gaps, the laminate is held centred between the two ground planes using PTFE spacers. The existence of the FR-4 laminate with a thickness of 0.8 mm slightly affects the uniformity of the relative permittivity of the dielectric in the control network. However, this discrepancy is overcome by optimizing the parameters of the control network using the design CAD tool.

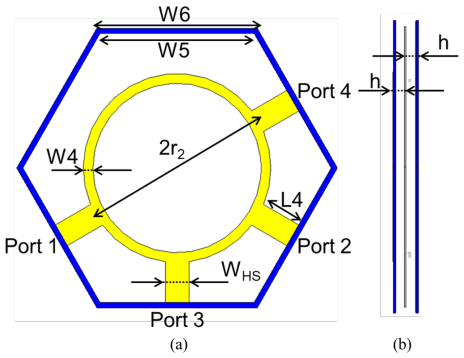

Figure 10. The proposed rat-race (**a**) front view (**b**) side view

Table 2. The parameters of the proposed control network (in mm)

Parameter	Value	Parameter	Value	Parameter	Value
W_4	6.5	r_2	120	$L6$	24
W_5	104	L_4	30	$L7$	140
W_6	108	$L5$	100	S	0.5

Figure 11 shows the simulated S-parameters of the proposed rat race. The return losses at any of its four ports its better than 25 dB at the desired frequencies. The signals at ports 1 and 2 have equal amplitudes with in-phase and out-of-phase

behaviours when fed from ports 3 and 4 respectively. Therefore, the Sum and Diff beams are created when port 3 and port 4 are excited while port 1 and port 2 are connected to *A1* and *A2* all respectively.

The current distributions across the proposed rat race at the desired frequencies are presented in Figure 12. It is clear that the signals at ports 1 and 2 are in-phase and out-of-phase when excited from ports 3 and 4 respectively. However, ports 3 and 4 are highly isolated from each other (better than 35 dB) which guarantees enough isolation between the Sum and Diff channels.

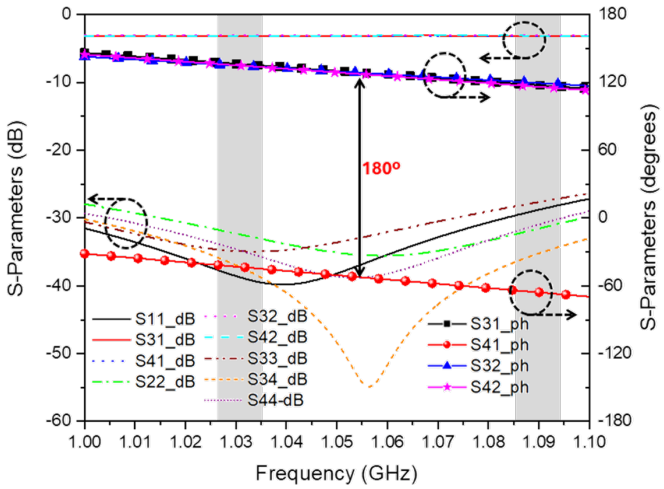

Figure 11. The simulated S-parameters of the proposed rat race

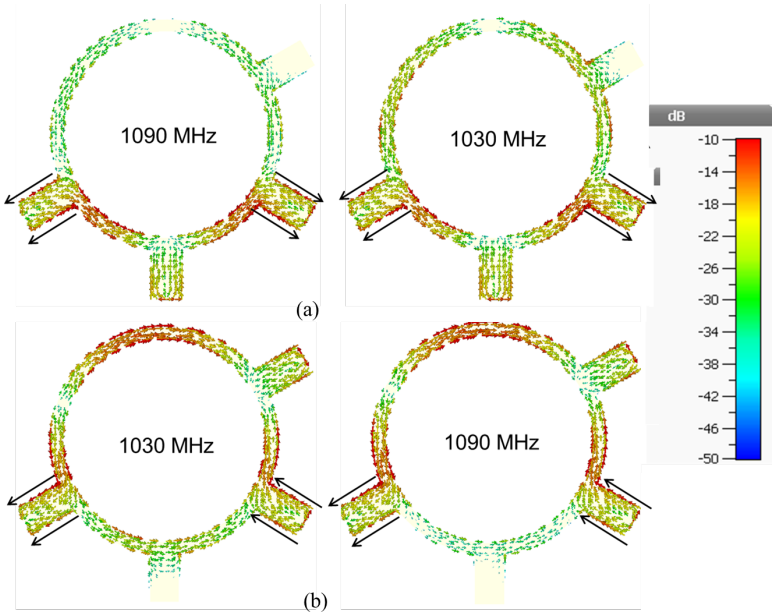

Figure 12. The current distributions across the proposed rat race when it is excited at (**a**) port 3 and (**b**) port 4

5.2 *The proposed directional coupler*

The proposed directional coupler is shown in Figure 13 and its dimensions are tabulated in Table 2. Its network is designed based on SL technology with air gaps as a dielectric. The network is made of copper with a thickness of 35 μm and printed on a rectangular-shaped FR-4 laminate with a thickness of 0.8 mm and a relative permittivity $\varepsilon_r \approx 4.3$ while the

ground planes are made from an aluminum sheet with a thickness of 3 mm. The thickness of the air gaps between the network and any of the two opposite ground planes is *h*. To keep the uniformity of the air gaps, the laminate is held centred between the two ground planes using PTFE spacers.

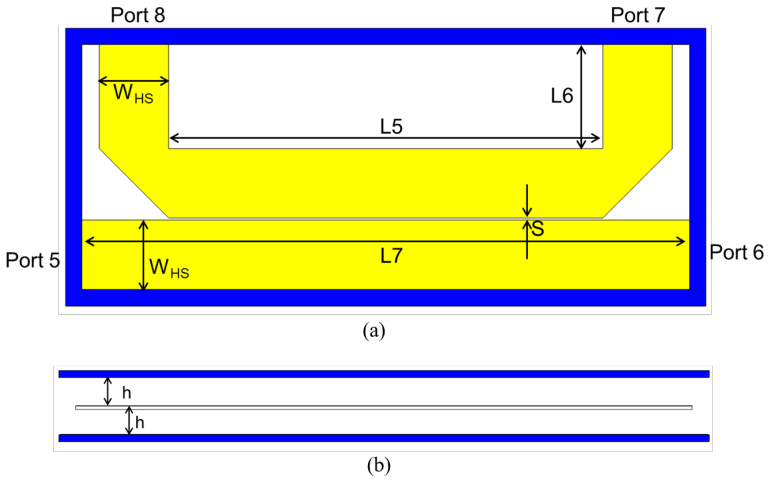

Figure 13. The proposed directional coupler (**a**) front view (**b**) side view

The S-parameters of the proposed directional coupler are shown in Figure 14. The signal at port 5 is directed to port 6 with an insertion loss of 0.6 dB and coupled to port 7 with a coupling coefficient of about 10 dB.

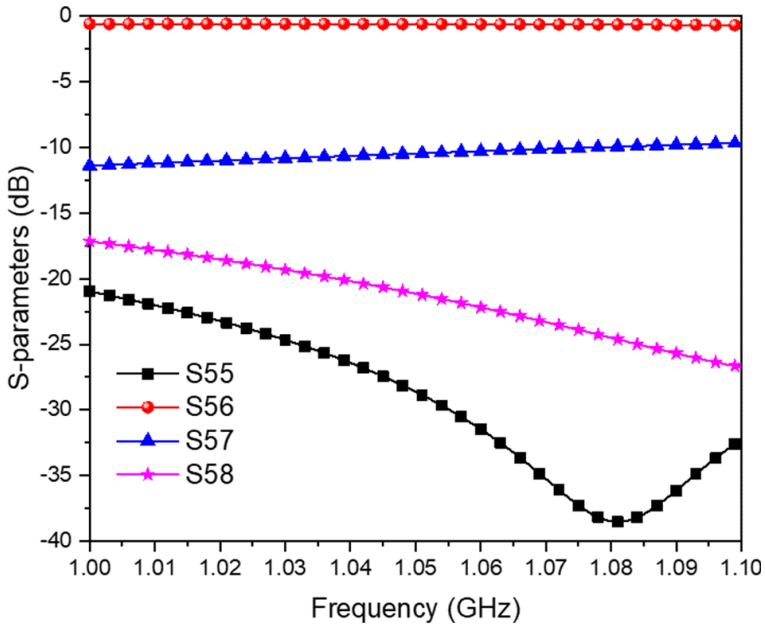

Figure 14. The simulated S-parameters of the proposed directional coupler

The full control network is shown in Figure 15. It consists of the proposed rat-race network merged with two identical copies of the proposed directional coupler (DC1 and DC2) where DC1 and DC2 are connected to the Sum and Diff ports (ports 3 and 4) of the rat-race, respectively.

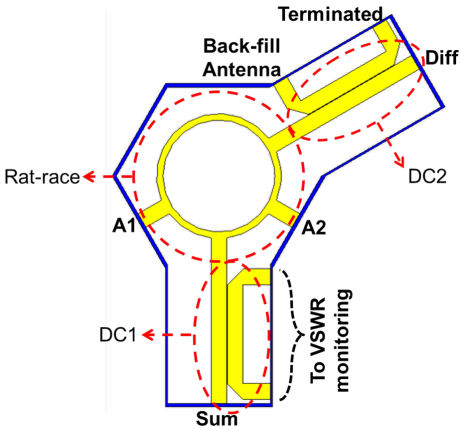

Figure 15. The proposed control network

The function of DC1 is to provide two different coupling ratios of the signal at the Sum port through the coupling ports (7 and 8). So, these coupling ratios may be used to measure and monitor the instant VSWR of the Sum channel. The function of DC2 is to provide a sample to the Diff signal from the backfill antenna through its 10-dB port. Therefore, the Diff beam is enhanced by adding a 10-dB sample from the signal transmitted (or captured) by the back-fill antenna, especially at the back lobe direction (the negative Z-axis) to guarantee its full coverage over the sidelobes of the Sum beam in all azimuth angles (especially at the back lobe).

The assembled proposed SSR antenna array is shown in Figure 16.

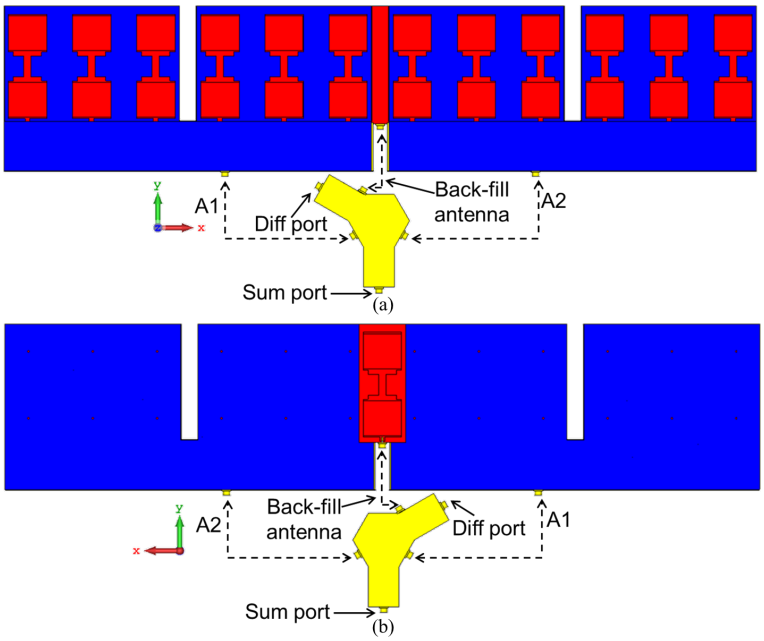

Figure 16. The assembled proposed SSR antenna array (**a**) front view (**b**) rear view

6. Prototyping and measurements

To validate the idea, a prototype of the whole SSR antenna has been fabricated and measured. Figure 17 shows the fabricated prototype and an assembled block diagram. The whole system has been measured using an Agilent Vector Network Analyzer (VNA) and an over-the-air (OTA) antenna measurement setup.

For a better understanding of the function of the assembled prototype, the transmission and reception processes of the two beams (Sum and Diff) can be described as follows:

1. Sum beam: the transmitted signal is fed to the Sum port of the control network (refer to Figure 15). The signal is split in phase and equally in magnitude through ports *A1* and *A2*. The in-phase signals travel to the arrays *A1* and *A2* through coaxial cables. Then, the arrays form the Sum beam with maximum constructive interference at the boresight. The whole process is reversed during reception.

2. Diff beam: the transmitted signal is fed to the Diff port of the control network (refer to Figure 15). A sample of it (10 dB) is coupled to the back-fill antenna port. This sample travels through a coaxial cable to the back-fill antenna which radiates the sample backwards. The remaining part of the transmitted signal is split out-of-phase and equally in magnitude through ports *A1* and *A2*. The out-of-phase signals travel to the arrays *A1* and *A2* through coaxial cables. Then, the arrays form the Diff beam with maximum destructive interference at the boresight. The whole process is reversed during reception.

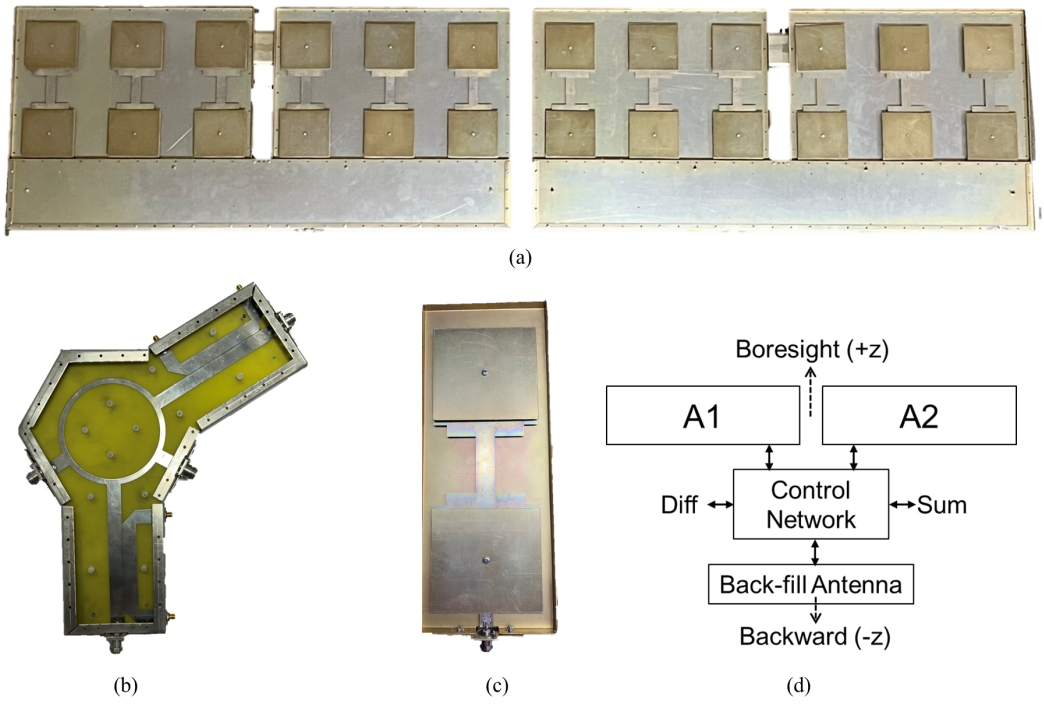

Figure 17. Prototype (**a**) A1 and A2 (**b**) the control network (**c**) the back-fill antenna (**d**) the assembled block diagram

The measured return losses of the antenna arrays *A1* and *A2* are shown in Figure 18a while the measured S-parameters of the whole control network are shown in Figure 18b. It is clear that the return losses, insertion losses and insertion phases satisfy the requirements of the design at the desired frequencies.

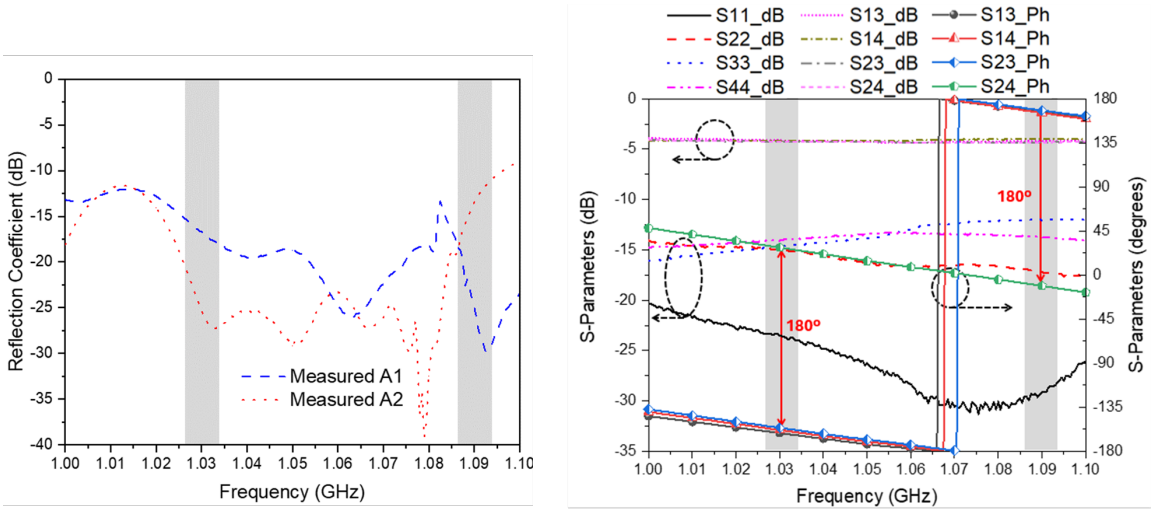

(a) (b)

Figure 18. The measured S-parameters of (**a**) Arrays A1 and A2 (**b**) control network

The simulated and measured radiation patterns across the H-plane at 1030 MHz and 1090 MHz are shown in Figure 19a,b respectively. It is clear that the side lobe level of the Diff beam is at least 5 dB more than the Sum beam in full azimuth coverage angles at both frequencies. So, these two beams (Sum and Diff) are enough to form the monopulse technique without the need for a third control beam like most of the reported designs in the literature. This highly reduces the complexity and cost of the utilized hardware and signal processing in the SSR and enhances its performance. The back lobe radiations observed in the measurements (Figure 19b) are significantly suppressed compared to the simulations (Figure 19a) . This discrepancy arises from the large concrete block, which is part of the tower structure used to fix the prototype during the measurements. The concrete block obstructs a substantial portion of the radiation, leading to the suppression of the back lobe pattern. The measured realized gains at the uplink and downlink frequencies are about 22.2 dBi.

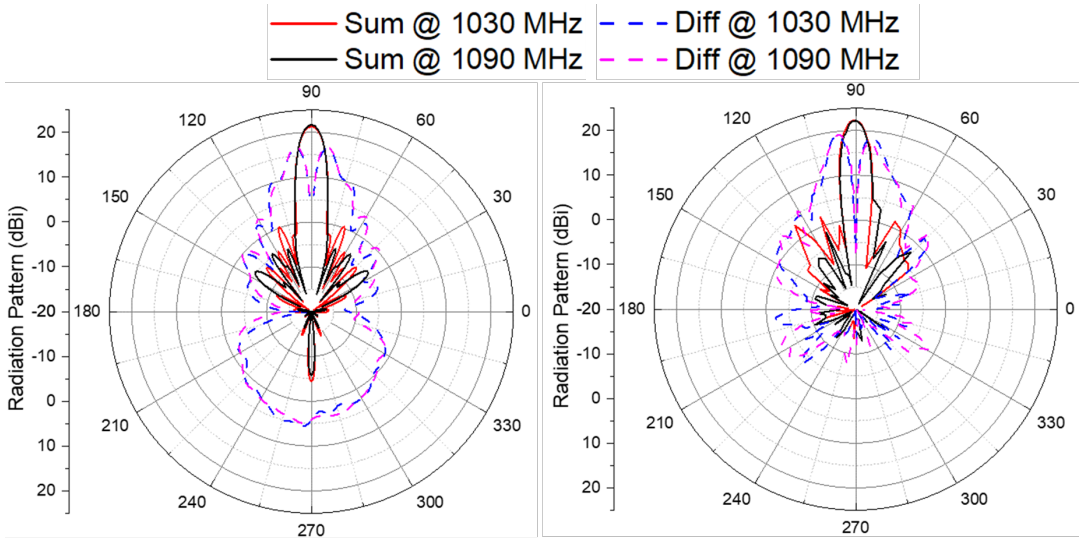

(a) (b)

Figure 19. The radiation patterns (**a**) simulated (**b**) measured

To evaluate the performance of the proposed design, a comparison to the state-of-the-art reported designs is tabulated in Table 3. It is evident that the proposed antenna is suitable to be employed with an SSR system with reduced complexity as it utilizes only two beams (Sum and Diff) to introduce a monopulse technique with a good Sum-to-Diff ratio at the boresight (30 dB) and full sidelobe coverage in all other azimuth angles. It also provides a sufficient gain with vertical polarization which is suitable for SSR applications with all results verified through practical measurements.

Table 3. A comparison to the state-of-the-art reported designs

Ref	Number of beams	Complexity	Gain (dBi)	Pol	Validation
[6]	3	Complex	27	V	Simulations
[7]	3	Complex	24	V	Measurements
[9]	2	Simple	18.5	V	Simulations
[10]	2	Simple	18	H	Simulations
[5]	3	Complex	NA	NA	Simulations
This Work	2	Simple	22.2	V	Measurements

The power-handling capability of an antenna in an SSR system is another important factor in evaluating the performance of the antenna. So, the proposed antenna has been tested through simulations to determine the maximum power level which could be handled.

Figure 20 shows the electric field distributions across the antenna array when it is fed by 1 W at its input ports. For simplicity, the electric field across *A1* only is presented. The power handling capability is calculated according to the square relationship between power and electric field intensity as [19, 20, 21]:

$$P_{\max} = \left(\frac{E_{br}}{E_{\max}}\right)^2 P_{in} \tag{4}$$

where:

P_{max}: the max power capacity

P_{in}: the input power (1 W in simulations)

E_{br}: vacuum breakdown threshold (7 MV/m at Lband [22])

E_{max}: the max electric field intensity when P_{in} is applied.

From Figure 20, the maximum electric field intensity is 4233 V/m when a 1 W input signal is applied. Therefore, Equation (4) numerically indicates that P_{max} is 2.7 MW which is far above the maximum utilized transmitted power in most of the SSR systems (typically a 150 to 1500 watts [4]).

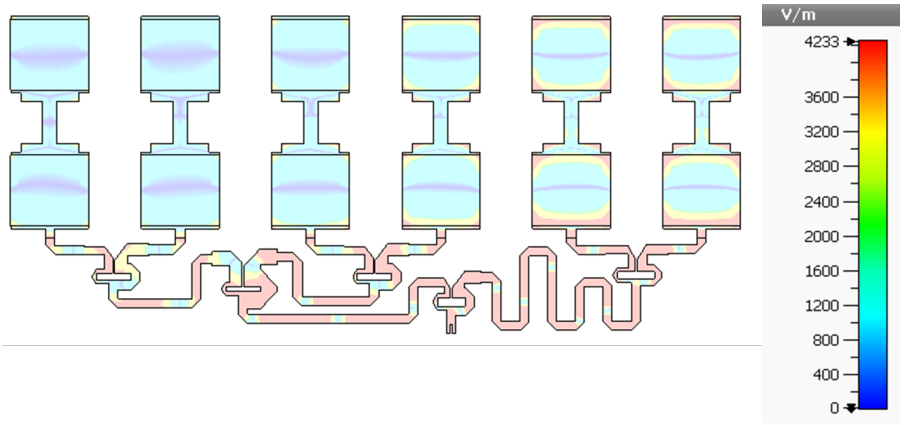

Figure 20. The electric field distributions across the proposed antenna array

7. Conclusions

A novel high-power monopulse antenna array has been proposed to be employed in an SSR system for long-range air traffic detection and control. The proposed antenna array has utilized a novel hybrid-strip technology to merge microstrip patch antennas with a stripline feeding network with good impedance matching and a minimal transition effect. The proposed antenna uses only two beams (Sum and Diff) to fully suppress the sidelobes in all azimuth angles and provides a Sum-to-Diff ratio of 30 dB at boresight. The antenna gain is 22.2 dBi with vertical polarization. The antenna can theoretically handle an input power of up to 2.7 MW. These results have proven that the proposed antenna array is an excellent candidate for an SSR system.

Conflict of interests

There is no conflict of interest declared by the authors.

References

[1] J. L. Volakis, *Antenna Engineering Handbook*. New York, NY, USA: McGraw-Hill, 2007.

[2] M. J. Alexander, "The Design and Performance of a Large Vertical Aperture Antenna for Secondary Surveillance Radar," *GEC Rev.*, vol. 4, no. 2, pp. 109–117, 1988.

[3] P. Bezousek and V. Schejbal, "Radar Technology in the Czech Republic," *IEEE Aerosp. Electron. Syst. Mag.*, vol. 19, pp. 27–34, 2004.

[4] T. Lutnaes, *Probability of Positive Identification with an IFF E-scan System*. Uppsala, Sweden: Uppsala University, 2018.

[5] V. Schejbal, P. Bezousek, J. Pidanic, and M. Chyba, "Secondary Surveillance Radar Antenna [Antenna Designer's Notebook]," *IEEE Antennas Propag. Mag.*, vol. 55, no. 2, pp. 164–170, Apr. 2013.

[6] T. Zalabsky and T. Hnilicka, "An Antenna Array Synthesis for Large Vertical Aperture Antenna for Secondary Surveillance Radar," in *Proc. 2017 Int. Symp. ELMAR*, Zadar, Croatia, Sept. 18–20, 2017, pp. 119–122.

[7] H. Aliakbarian, M. Khak, M. Shahpari, A. N. Yeganeh, F. Mazlumi, S. H. Najmolhoda, et al., "An Efficient Multi-Beam Array Architecture for L-Band Secondary Surveillance Radars," *Radio Eng.*, vol. 28, no. 1, p. 85, 2019.

[8] M. N. Jazi, G. Askari, H. Eskandari, and H. M. Sadeghi, "Design and Implementation of an Aperture Coupled Microstrip IFF Antenna," *Int. J. Inform. Commun. Technol.* , vol. 1, pp. 13–19, 2009.

[9] M. Hedayati, G. Askari, P. Moslemi, and H. M. Sadeghi, "Design and Implementation of a Planar Slot Antenna for SSR," in *Proc. Prog. Electromagn. Res. Symp.*, Prague, Czech Republic, Jul. 6–9, 2015.

[10] M. Abdolahi, Z. Pourgholamhossein, H. M. Sadeghi, and M. Fadaei, "Design and Analysis Performance of a New Patch Array Antenna for SSR," in *Proc. Prog. Electromagn. Res. Symp.(PIERS)*, St. Petersburg, Russia, May 22–25, 2017.

[11] R. Rimolo-Donadio, J. Supper, T. -M. Winkel, H. Harrer, and C. Schuster, "Analysis and Mitigation of Parasitic Mode Conversion for Microstrip to Stripline Transitions," *IEEE Trans. Electromagn. Compat.*, vol. 54, no. 2, pp. 495–498, Apr. 2012.

[12] M. Leib, M. Mirbach, and W. Menzel, "An Ultra-Wideband Vertical Transition from Microstrip to Stripline in PCB Technology," in *Proc. 2010 IEEE Int. Conf. Ultra-Wideband*, Nanjing, China, Sept. 20–23, 2010, pp. 1–4.

[13] J. Chramiec and B. J. Janiczak, "Design of Impedance-Transforming Microstrip-Balanced Stripline Tapered Transitions," *IET Electron. Lett.*, vol. 29, pp. 3–4, 1993.

[14] A. Gámez-Machado, D. Valdés-Martín, A. Asensio-López, and J. Gismero-Menoyo, "Microstrip-to-Stripline Planar Transitions on LTCC," in *Proc. 2011 IEEE MTT-S Int. Microw. Workshop Ser. Millimeter Wave Integration Technol.*, Sitges, Spain, Sept. 15–16, 2011, pp. 1–4.

[15] C. K. Queck and L. E. Davis, "Microstrip and Stripline Ferrite-Coupled-Line (FCL) Circulators," *IEEE Trans. Microw. Theory Tech.*, vol. 50, no. 12, pp. 2910–2917, Dec. 2002.

[16] D. M. Pozar, *Microwave Engineering*, 4th ed. Hoboken, NY, USA: John Wiley & Sons, 2011.

[17] A. Alieldin, Y. Huang, M. Stanley, S. D. Joseph, and D. Lei, "A 5G MIMO Antenna for Broadcast and Traffic Communication Topologies Based on Pseudo Inverse Synthesis," *IEEE Access*, vol. 6, pp. 65935–65944, 2018.

[18] J. Ansari, P. Singh, N. P. Yadav, and B. Vishvakarma, "Analysis of Shorting PIN Loaded Half Disk Patch Antenna for Wideband Operation," *Prog. Electromagn. Res. C*, vol. 6, pp. 179–192, 2009.

[19] A. Eid, A. Alieldin, A. El-Akhdar, A. El-Agamy, W. Saad, and A. Salama, "A Novel High Power Frequency Beam-Steering Antenna Array for Long-Range Wireless Power Transfer," *Alexandria Eng. J.*, vol. 60, no. 2, pp. 2707–2714, 2021.

[20] M. Akmal, A. Alieldin, and A. R. Eldamak, "A High-Power Sandwiched Omnidirectional Circularly Polarized Antenna for GNSS Systems," *IEEE Access*, vol. 11, pp. 31167–31176, 2023.

[21] R. Meng, Y. Xia, Y. Guo, and Q. Zhu, "An X-Band 48-Way Leaky Waveguide Antenna with High Aperture Efficiency and High Power Capacity," *IEEE Trans. Antennas Propag.*, vol. 66, no. 12, pp. 6799–6809, Dec. 2018.

[22] A. Semnani, A. Venkatraman, A. Alexeenko, and D. Peroulis, "Frequency Response of Atmospheric Pressure Gas Breakdown in Micro/Nanogaps," *Appl. Phys. Lett.*, vol. 103, no. 6, p. 3102, 2013.